JOURNAL OF MATERIALS SCIENCE **37** (2002) 4793–4799

# The characterization of thermal and elastic constants for an epoxy photoresist SU8 coating

R. FENG, R. J. FARRIS*
*Polymer Science and Engineering Department, University of Massachusetts Amherst, Amherst, MA 01003, USA*
*E-mail: rjfarris@polysci.umass.edu*

All of the thermal and elastic constants of the high-aspect ratio, negative, UV resist, SU8 coating were carried out, and the compliance matrix of the coating was obtained. DSC, TGA, TMA, and DMTA techniques were utilized to study the thermal properties of the material. The in-plane thermal expansion coefficient (TEC) ($\alpha_1$) was determined by TMA, and the glass transition behavior was studied by DMTA. The TGA study provided information about the thermal stability of the material, and DSC was applied to study the thermal calorimetric properties of the material. The in-plane Young's modulus ($E_1$) was measured by tensile tests. The residual stresses of a 1D stretched ribbon sample and a 2D stretched membrane sample were measured by vibrational holography tests, and the in-plane Poisson's ratio ($\nu_1$) was also determined by holography. The out-of-plane Poisson's ratio ($\nu_2$) was obtained by high pressure gas dilatometry measurements. The bulk compressibility ($\kappa$) and the volumetric TEC ($\alpha_v$) of the material were measured by a pressure-volume-temperature (PVT) apparatus. Finally, the out-of-plane properties, including the out-of-plane TEC ($\alpha_2$) and the out-of-plane Young's modulus ($E_2$), were calculated from the measured in-plane properties and the volumetric properties. Therefore, the compliance matrix of the studied SU8 coating could be obtained. 

## 1. Introduction

SU8 epoxy is a negative photoresist, which is usually utilized in ultrathick, high-aspect-ratio micro-electrical mechanical systems (MEMS) type applications [1–3]. Examples are sensor actuators and molds for electroplating gears and coils. SU8 can also be used in other applications such as bonding pads and UV cured packaging materials. The SU8 resist is based on epoxy resin technology, which possesses good adhesion characteristics superior to conventional thick resists. SU8 epoxy has sensitivity in the near UV, 365 nm, E-beam, and X-ray regions. The optical absorption in the UV region allows near vertical sidewall profiles in thick coatings, and an aspect ratio of 20:1 has been achieved.

The epoxy resin has first been dissolved in an organic solvent to form a concentrated solution, which can then be coated onto a rigid substrate to form thick coatings. The following processing steps include: soft baking to remove the solvent; UV exposure to create the acid catalyst; thermal baking to form a network structure after crosslinking. The properties of the material are found to be sensitive to the processing conditions [4]. In order to exploit the potential of the material, the process dependent mechanical and thermal properties must be understood. To our knowledge, only a few studies have been undertaken to determine the thermal and mechanical properties of SU8. Lorenz [3, 5, 6] determined the bi-axial elastic modulus and the thermal expansion coefficient (TEC) by measuring the bow response of a 20 $\mu$m thick resist layer on both Al and Si substrates after being subjected to a thermal cycling ($\Delta T = 75^{\circ}$C). The resultant bi-axial modulus was 5.18 GPa, and the TEC was 52 ppm/°C. Lorenz also measured the friction coefficient $\mu$ on a pin-on-disc installation, with a disc rotation of 10 rpm and a load of 10 g, yielding a $\mu$ value of 0.19. A modulus of elasticity in tension of 4.02 GPa was measured by tensile testing [7]. One advantage of the material is its good thermal stability. The glass transition temperature ($T_g$) is higher than 200°C, and the degradation temperature ($T_d$) is about 380°C [8]. So far, no properties for the thickness direction have ever been reported. The material is usually treated as isotropic in all three directions, since the properties in the thickness direction are too difficult to measure. However, great in-plane stress can be created during the baking processing, therefore, the material only has a transversely isotropic symmetry.

In the small-strain and linear-elastic region, a generalized Hooke's law can be applied to describe the materials response. For a transversely isotropic material, there are five independent elastic compliances and two TECs in the equation, as shown in Scheme 1 [9]. The directions **1** and **2** are in the coating plane, and direction **3** is the perpendicular to the plane of the coating.

*Author to whom all correspondence should be addressed.

$$\begin{bmatrix} \varepsilon_{11} - \alpha_1 \Delta T \\ \varepsilon_{22} - \alpha_1 \Delta T \\ \varepsilon_{33} - \alpha_2 \Delta T \\ 2\varepsilon_{23} \\ 2\varepsilon_{13} \\ 2\varepsilon_{12} \end{bmatrix} = \begin{bmatrix} C_{11} & C_{12} & C_{13} & 0 & 0 & 0 \\ C_{12} & C_{11} & C_{13} & 0 & 0 & 0 \\ C_{13} & C_{13} & C_{33} & 0 & 0 & 0 \\ 0 & 0 & 0 & 2(C_{11} - C_{12}) & 0 & 0 \\ 0 & 0 & 0 & 0 & C_{55} & 0 \\ 0 & 0 & 0 & 0 & 0 & C_{55} \end{bmatrix} \begin{bmatrix} \sigma_{11} \\ \sigma_{22} \\ \sigma_{33} \\ \sigma_{12} \\ \sigma_{13} \\ \sigma_{12} \end{bmatrix}$$

$$C_{11} = 1/E_1 \qquad C_{12} = -\nu_1/E_1 \qquad C_{55} = 1/G_2$$
$$C_{33} = 1/E_2 \qquad C_{13} = -\nu_2/E_1$$

$\varepsilon_{ij}$ : Strain — $E_{ij}$ : Tensile modulus
$\sigma_{ij}$ : Stress — $G_{ij}$ : Shear modulus
$\nu_{ij}$ : Poisson's ratio — $C_{ij}$ : Compliance
$\alpha_i$ : Thermal expansion coefficient (TEC)

*Scheme 1* Generalized Hooke's law for a transversely isotropic material.

Due to the thickness of thin coatings, the out-of-plane properties cannot be measured by the methods used for the in-plane properties determination. During the past decade, some very powerful methods of fully characterizing all of the elasticity coefficients for thin polymeric films and coatings have been developed in our laboratory [10–13]. These are direct, albeit somewhat complicated, mechanical methods to give the full set of elasticity coefficients, which include two normal compliances, two Poisson's ratios, two shear moduli and two TECs for a transversely isotropic material. The special techniques involved in this characterization include vibrational holographic interferometry, high-pressure gas dilatometery, pressure-volume-temperature (PVT) apparatus, and torsion pendulum. The theory and applications of these techniques have been reported elsewhere [10–13] so only a brief introduction about those techniques is given in this paper.

## 2. Experiments

### 2.1. Material

The SU8 coating used in this study was provided by the Hewlett-Packard Company. SU8 epoxy was first coated onto a gold coated silicon wafer substrate, followed by a lithography process. Samples with the desired shape (blanket, dogbone, and strip) and dimensions were obtained by choosing the appropriate masks during UV exposure. To peel the SU8 samples off the substrate, the wafers were immersed into $KI/I_2$ solution. SU8 samples were set free after the gold reacted with the solution under mild conditions. The thickness of the coating was measured by a Veeco Metrology Dektak $D_3$ Profilometer, and was about 30 $\mu$m. The density of the sample was measured by a standard density column, and the result was 1218 kg/m$^3$.

### 2.2. Thermal analysis

A TA instruments Thermal–Mechanical Analyzer (TMA 2940) was applied to measure the dimensional stability of the material. A small force, 0.01 N, was applied to the strip sample to prevent wrinkling when the dimension of the sample was measured. A heating scan rate of 5°C/min was applied unless otherwise indicated. A nitrogen purge of $6 \times 10^{-5}$ m$^3$/min was used to prohibit sample oxidation during heating. The TEC was calculated from the second heating or cooling scan, since the first heating scan included information about the thermal and stress history of the material.

Thermal degradation and weight-loss studies were carried out using a TA instruments Thermogravimetric Analyzer (TGA 2950). The tested temperature range was from room temperature to 1000°C with a heating rate of 10°C/min. The experiment was performed under the protection of nitrogen with a flow rate of $10^{-4}$ m$^3$/min.

Thermal calorimetric properties of the material were studied using a TA instruments Differential Scanning Calorimeter (DSC2910). All the measurements were carried out under a nitrogen purge with a ramp rate of 10°C/min.

The glass transition behavior of the samples was studied using a Rheometric Scientific DMTA IV system. Samples, ca. $10 \times 5$ mm, processed under different conditions were tested in an oscillatory tensile mode by scanning from 25°C to 350°C at a rate of 1°C/min and a frequency of 1 Hz.

### 2.3. Tensile tests

Strip samples with dimension of $70 \times 5$ mm were used for tensile tests. An Instron model 5564 with 1 kN load cell was applied to perform the measurements. The crosshead speed was 5 mm/min. At least ten specimens were tested and the average value was reported.

### 2.4. Poisson's ratio measurements

#### *2.4.1. In-plane Poisson's ratio ($\nu_1$)*

The in-plane Poisson's ratio was measured by the vibrational holography technique. As shown in Fig. 1, 2D stretched circular membrane sample was made from the blanket specimens, and the 1D stretched sample was made from the strip specimens. The resonant frequencies of the 1D stretched ribbon sample and the 2D stretched circular membrane sample were measured by holographic interferometry, and the 1D stress and 2D stress were calculated. The in-plane Poisson's ratio could then be calculated from these data.

#### *2.4.2. Out-of-plane Poisson's ratio ($\nu_2$)*

The out-of-plane Poisson's ratio could be obtained from high pressure gas dilatometry measurements. A strip sample was held under constant strain condition in a high pressure chamber. The change in stress as a function of hydrostatic pressure from 0 MPa to 17 MPa was examined under nitrogen gas. By plotting the stress change vs. temperature, the slope yielded $1 - \nu_1 - \nu_2$.

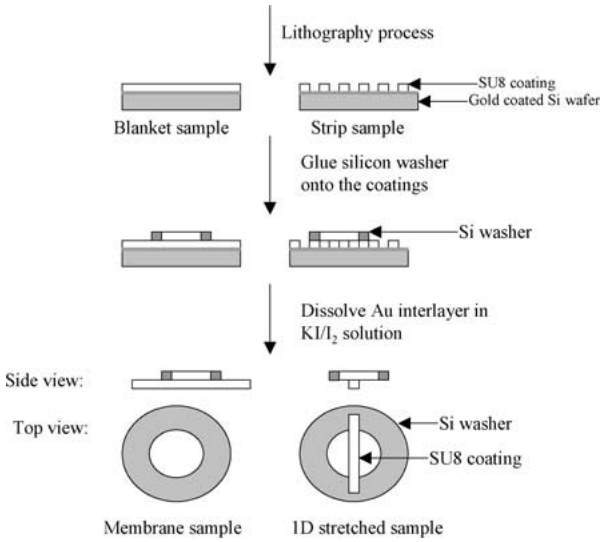


*Figure 1* Sample preparation for holography measurements.

Since $\nu_1$ had been determined by holography, $\nu_2$ could then be obtained from this measurement.

## 2.5. Bulk properties

The bulk properties of the material, including bulk compressibility, $\kappa$, and volumetric TEC, $\alpha_v$, were measured by PVT experiments. About 1 gram of SU8 sample was stacked and placed into the rigid sample cell. The void space was then filled with mercury by a specially designed filling apparatus. The temperature of the sample was measured by a thermocouple and controlled by a heating jacket. The pressure was controlled by an Enerpac P-2282 hand pump. The change in the sample volume was detected by the movement of a linear-variable-differential-transformer (LVDT), which was connected with a flexible bellows at the bottom of the sample cell. The volume change of the sample, as a function of pressure and temperature, was measured precisely. The isothermal run was carried out over a temperature range of 30°C to 160°C, with the pressure changing from 10 MPa to 90 MPa at an interval of 5 MPa.

## 2.6. Shear modulus

The out-of-plane shear modulus, $G_2$, was measured by a torsion pendulum. To minimize the test error, very narrow ribbon samples were required. One end of the sample was fixed, and the other end was attached to a circular disk. The disk was first twisted to a small angle and then released. The period of the oscillation, which is related to the out-of-plane shear modulus of the material, was measured.

# 3. Results and discussion

## 3.1. Thermal properties

Fig. 2 shows the DSC curve of the material. The huge exothermal peak at the first heating scan indicates that the material was not fully crosslinked after the processing. The exothermal peak disappeared in the second heating scan, which implied that the crosslinking reaction could be completed when being heated to 350°C during the first DSC scan.

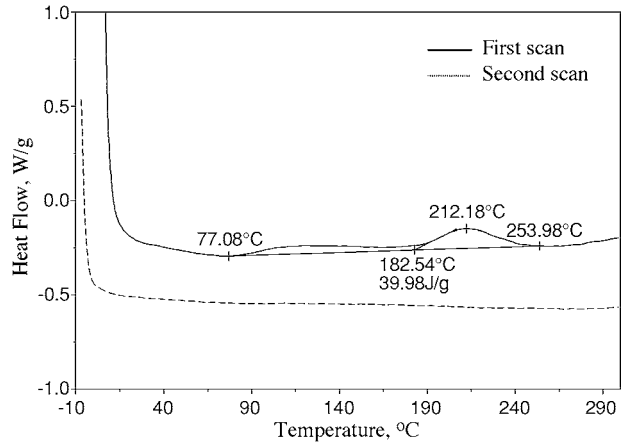


*Figure 2* DSC curves of the SU8 coating.

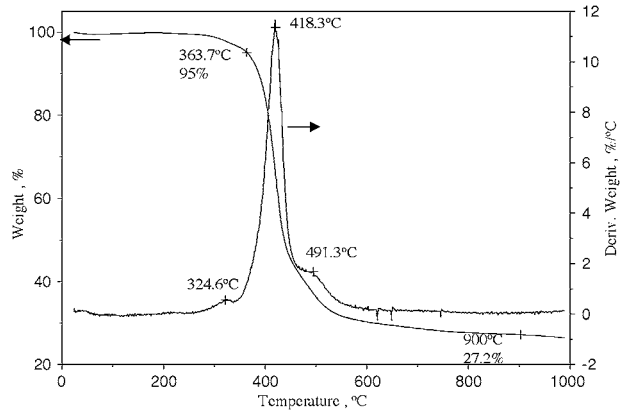


*Figure 3* TGA curves of the SU8 coating.

The thermal stability of the material was studied by TGA. Fig. 3 shows the TGA behavior of the SU8 coating. The temperature at 5% weight loss was about 360°C and the char yield at 900°C was around 27%. However, it should be pointed out that the degradation reported in this paper is the behavior of the material under the protection of nitrogen.

The in-plane TEC, $\alpha_1$, and the dimensional stability of the samples were studied by TMA. Fig. 4 shows the dimension change with the temperature. $\alpha_1$ was calculated from the slope of the second heating scan at a temperature range of [60°C, 120°C]:

$$\alpha_1 = 87.1 \text{ ppm/°C}$$

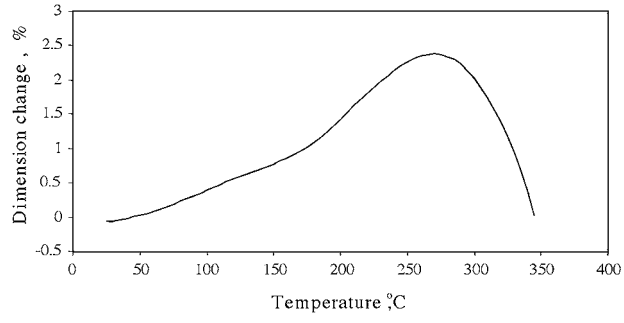


*Figure 4* Dimension change with temperature of the SU8 coating.

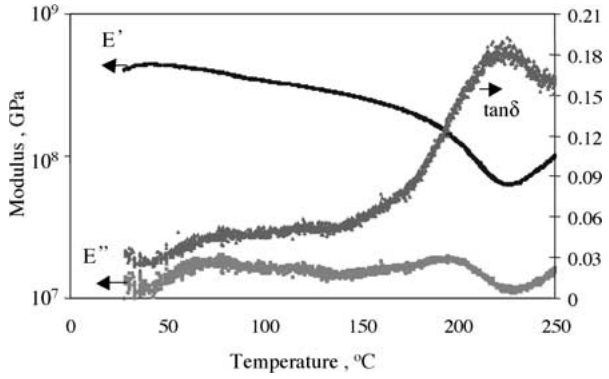


*Figure 5* DMTA curves of the SU8 coating.

The shrinkage temperature of the coating, which is dictated by the thermal history of the material, is about 270°C under the processing conditions used in this paper.

The glass transition behavior of the material was studied by DMTA and the plots are shown in Fig. 5. The $\alpha$ peak, which is taken as the glass transition temperature in this study, appears at about 220°C. One important feature of these plots is the broadness of the $\alpha$ peak. This indicated an inhomogeneous local composition of the material.

## 3.2. Poisson's ratio measurement

### *3.2.1. In-plane Poisson's ratio ($\nu_1$)*

Due to the mismatch in TEC between the substrate and the polymeric coating, and also because of volumetric change of the coatings caused by chemical reaction and the evaporation of the solvent, great residual stress can be created in the system during the processing. By taking advantage of the residual stress trapped in the system during the process, 2D stretched membrane sample and 1D stretched sample were made for holographic tests. The original state of stress in the coating were kept the same by the way we prepared the samples, so that the 1D and 2D stress for the sample, being processed under the exact same conditions, could be determined.

For a circular membrane, the 2D stress related with the resonant frequency by [10–15]:

$$\sigma^{2D} = 4\rho\pi^2 R^2 \left(\frac{f_{ni}}{Z_{ni}}\right)^2 \tag{1}$$

where, $\sigma^{2D}$ is the 2D stress of the membrane sample (MPa); $R$ is the radius of the circular sample (m); $\rho$ is the density of the sample (kg/m$^3$); $f_{ni}$ is the resonant frequency of vibration (kHz); $Z_{ni}$ is the $i$th zero of $n$th order of Bessel function.

For a 1D stretched ribbon sample,

$$\sigma^{1D} = 4\rho L^2 \left(\frac{f_i}{i}\right)^2 \tag{2}$$

where, $\sigma^{1D}$ is the 1D stress of the ribbon sample (MPa); $L$ is the length of the ribbon sample (m); $f_i$ is the resonant frequency for $i$th mode (kHz).

TABLE I In-plane Poisson's ratio measurements

| 2D stress (MPa) | | | | 1D stress (MPa) | | | |
|---|---|---|---|---|---|---|---|
| $m$ | $n$ | $F_{mn}$ (kHz) | $\sigma^{2D}$ (MPa) | $i$ | $F_i$ (kHz) | $\sigma^{1D}$ (MPa) | $\nu_1$ |
| 0 | 1 | 2.919 | 26.0 | 1 | 1.623 | 17.46 | |
| 1 | 1 | 4.387 | 25.7 | 2 | 3.250 | 17.03 | |
| 2 | 1 | 6.453 | 23.4 | 3 | 4.528 | 15.12 | 0.33 |
| 3 | 1 | 8.234 | 24.3 | 5 | 7.887 | 16.63 | |
| 4 | 1 | 9.726 | 23.9 | 7 | 12.25 | 16.60 | |
| | | Average = 24.7 | | | | Average = 16.6 | |

For a biaxially stretched membrane sample, the following constitutive equation was satisfied:

$$\begin{bmatrix}\varepsilon^{2D}\\ \varepsilon^{2D}\end{bmatrix} = \begin{bmatrix}C_{11} & C_{12}\\ C_{12} & C_{11}\end{bmatrix}\begin{bmatrix}\sigma^{2D}\\ \sigma^{2D}\end{bmatrix}$$

or

$$\varepsilon^{2D} = C_{11}\sigma^{2D} + C_{12}\sigma^{2D} \tag{3}$$

For the 1D stretched strip sample processed under the same conditions,

$$\varepsilon^{1D} = C_{11}\sigma^{1D} \tag{4}$$

$$\varepsilon_{11}^{2D} = \varepsilon_{11}^{1D}$$

$$C_{11}\sigma^{2D} + C_{12}\sigma^{2D} = C_{11}\sigma^{1D} \tag{5}$$

The in-plane Poisson's ratio could then be calculated by:

$$\nu_1 = \frac{C_{12}}{C_{11}} = \frac{\sigma^{2D} - \sigma^{1D}}{\sigma^{2D}} \tag{6}$$

Table I summarized the results of the in-plane Poisson's ratio measurements. The main error in the Poisson's ratio measurements comes from the 1D stress measurement. Since the coating can be very fragile, it was difficult to cut the membrane sample into ribbon sample as we usually do in Poisson's ratio measurements [4, 10–13]. Strip samples processed under the same conditions as the blanket sample was used to make the 1D stretched sample instead.

### *3.2.2. The out-of-plane Poisson's ratio ($\nu_2$)*

The out-of-plane Poisson's ratio was measured by high pressure gas dilatometry [16]. For a uniaxially stretched ribbon sample under hydrostatic pressure, $P$, we have:

$$\varepsilon_{11} = C_{11}\sigma_{11} + C_{12}\sigma_{22} + C_{13}\sigma_{33} \tag{7}$$

Since,

$$\sigma_{11} = \sigma - P \quad \text{and} \quad \sigma_{22} = \sigma_{33} = -P \tag{8}$$

By inserting Equation 8 into Equation 7, Equation 7 could be rearranged into:

$$\frac{\varepsilon_{11}}{C_{11}} = \sigma - P\left(1 + \frac{C_{12}}{C_{11}} + \frac{C_{13}}{C_{11}}\right) \tag{9}$$

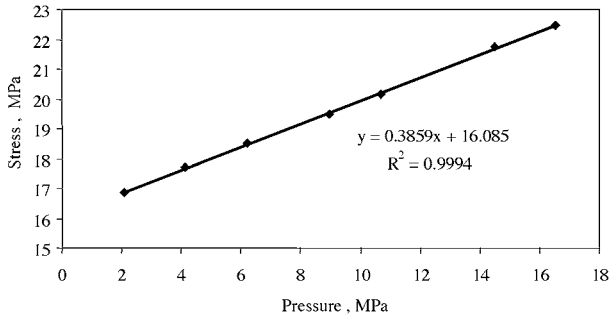


*Figure 6* High pressure gas dilatometry measurements.

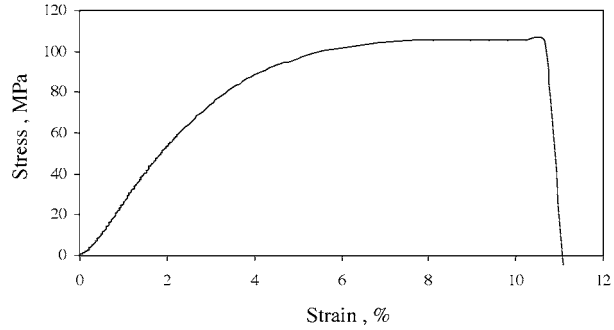


*Figure 7* A stress–strain curve of the SU8 coating.

Differentiating the equation with respect to pressure yields

$$\left(\frac{\partial \sigma}{\partial P}\right)_{\varepsilon_{11}} = 1 - \nu_1 - \nu_2 \tag{10}$$

By plotting the stress change vs. pressure, the slope yielded $1 - \nu_1 - \nu_2$. Since $\nu_1$ had been determined by holography, $\nu_2$ could then be calculated from Equation 10. Fig. 6 shows the relationship between the hydrostatic pressure and the stress of the sample.

$$\text{Slope} = 0.38$$

So

$$\nu_2 = 0.29$$

### 3.3. Tensile properties

The tensile test results of the SU8 coatings are shown in Table II. The in-plane Young's modulus was determined to be: $E_1 = 3.2 \pm 0.2$ GPa. The material is rather fragile after the processing. The elongation at break is around 8%. A stress–strain curve of the SU8 coating is shown in Fig. 7.

### 3.4. Shear modulus

The in-plane shear modulus, $G_1$, related with the in-plane Young's modulus and the Poisson's ratio by equation:

$$G_1 = \frac{E_1}{2(1 + \nu_1)} \tag{11}$$

Inserting the measured $E_1$ and $\nu_1$ into Equation 11, yielded:

$$G_1 = 1.2 \text{ GPa}.$$

The out-of-plane shear modulus, $G_2$, was then determined by torsion pendulum. Since the period of oscillation of the pendulum related with $G_2$ by [17, 18]

$$p^{-2} = \frac{8a^3 b G_2}{\pi^6 I L} \sum_{m=1}^{\infty} \frac{1}{m^4}\left(1 - \frac{1}{Q_m}\tanh Q_m\right) \tag{12}$$

$$Q_m = \frac{\pi b m}{2a}\sqrt{\frac{G_1}{G_2}} \tag{13}$$

where $p$ is the period of oscillation (s); $a$ is the width of sample (m); $b$ is the thickness of sample (m); $L$ is the length of sample (m); $I$ is the moment of inertia of the disc ($\text{kg} \cdot \text{m}^2$).

$G_2$ can be obtained by measuring the period of the oscillation of the pendulum, and the experimental result is shown in Table III.

### 3.5. Bulk properties

According to linear elasticity theory, the relationship for normal stress and strain for a transversely isotropic material can be written as:

$$\begin{aligned}
\varepsilon_{11} - \alpha_1 \Delta T &= C_{11}\sigma_{11} + C_{12}\sigma_{22} + C_{13}\sigma_{33} \\
\varepsilon_{22} - \alpha_1 \Delta T &= C_{12}\sigma_{11} + C_{11}\sigma_{22} + C_{13}\sigma_{33} \\
\varepsilon_{33} - \alpha_2 \Delta T &= C_{13}\sigma_{11} + C_{13}\sigma_{22} + C_{22}\sigma_{33}
\end{aligned} \tag{14}$$

For a sample under hydrostatic pressure, $\sigma_{11} = \sigma_{22} = \sigma_{33} = -P$, the dilatation of the total volume is by definition the sum of the strains in all three directions, which could be presented as a function of the temperature and pressure.

$$\frac{\Delta V}{V} = (2\alpha_1 + \alpha_2)\Delta T - P \sum_{i,j=1}^{3} C_{ij} \tag{15}$$

so:

$$-\frac{1}{V_0}\left(\frac{\partial V}{\partial P}\right)_T = \sum_{i,j=1}^{3} C_{ij} = \kappa \tag{16}$$

TABLE II Tensile properties of the SU8 coating

| Properties | Modulus (GPa) | Strength (MPa) | Elongation at break (%) |
|---|---|---|---|
| Value | $3.2 \pm 0.2$ | $106 \pm 3$ | $8 \pm 1$ |

TABLE III Out-of-plane Shear modulus measurement

| $a$ ($\mu$m) | $b$ ($\mu$m) | $L$ (mm) | Period (s) | $G_1$ (GPa) | $G_2$ (GPa) |
|---|---|---|---|---|---|
| 45.54 | 30 | 40.86 | 32.37 | 1.21 | 0.30 |

and

$$\frac{1}{V_0}\left(\frac{\partial V}{\partial T}\right)_P = 2\alpha_1 + \alpha_2 = \alpha_V \tag{17}$$

Finally, the out-of-plane TEC ($\alpha_2$)could be calculated by:

$$\alpha_2 = \alpha_v - 2\alpha_1 \tag{18}$$

and the out-of-plane Young's modulus could be obtained from:

$$\frac{1}{E_2} = \kappa - \frac{2}{E_1}(1 - \nu_1 - 2\nu_2) \tag{19}$$

Fig. 8 gives the specific volume change of the sample as a function of the pressure and temperature. The bulk compressibility, $\kappa$, and the volumetric TEC, $\alpha_v$, could be calculated from the data. Fig. 9 illustrates the relationship between the bulk compressibility and the temperature. The bulk compressibility increased almost linearly with the temperature in the experimental temperature range. The volumetric TECs at different pressures are plotted in Fig. 10, and the $\alpha_v$ at one atmosphere is obtained by extra-plotting.

$$\alpha_v = 452\,\text{ppm}/^\circ\text{C}$$
$$\kappa = 0.17\,(\text{GPa})^{-1}$$

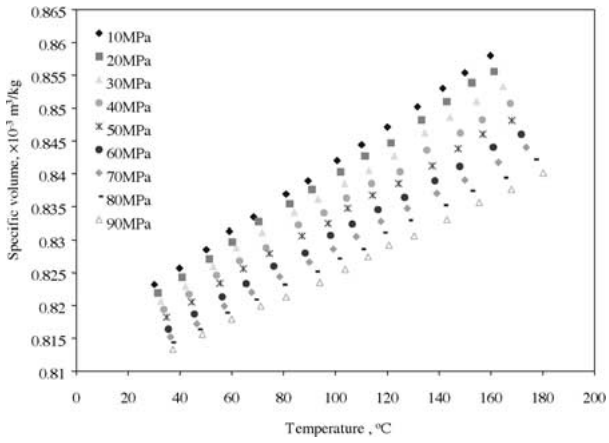


*Figure 8* PVT behavior of the SU8 coating.

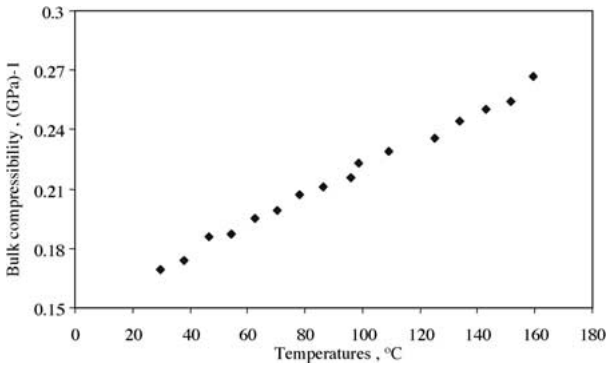


*Figure 9* The relationship between the bulk compressibility and the temperature.

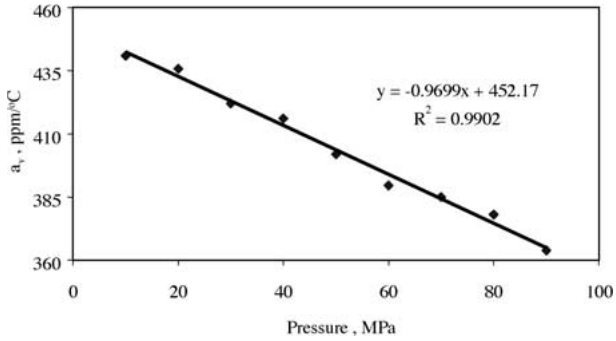


*Figure 10* Calculation of $\alpha_v$ at one atmosphere.

So:

$$\alpha_2 = 278\ \text{ppm}/^\circ\text{C}$$
$$E_2 = 5.9\ \text{GPa}$$

## 4. Summary

Finally, the compliance matrix of the SU8 coating was obtained:

$$[c_{ij}] = \begin{bmatrix} 0.31 & -0.10 & -0.09 & 0 & 0 & 0 \\ -0.10 & 0.31 & -0.09 & 0 & 0 & 0 \\ -0.09 & -0.09 & 0.17 & 0 & 0 & 0 \\ 0 & 0 & 0 & 0.82 & 0 & 0 \\ 0 & 0 & 0 & 0 & 3.3 & 0 \\ 0 & 0 & 0 & 0 & 0 & 3.3 \end{bmatrix}$$

The theoretical requirements for positive-definite energy criteria for a matrix of elastic constants include the following, all of which were satisfied by the above matrix.

1. $C_{11}, C_{22}, C_{33} > 0$
2. $C_{11}C_{22} - C_{12}^2 = 0.045 > 0$
3. $C_{11}C_{33} - C_{13}^2 = 0.055 > 0$
4. $C_{22}C_{33} - C_{23}^2 = 0.051 > 0$
5. Det $[C_{ij}] > 0$

All of the measured thermal and elastic constants of the SU8 coating and the experimental error for each value are summarized in Table IV. Due to the error accumulation effect, the out-of-plane constants have a higher degree of uncertainty when compared with the in-plane properties.

The good thermal stability and the mechanical properties of SU8 make it useful in thick and ultra thick

TABLE IV Thermal and elastic constants of the SU8 coating

| Constants | | Value |
|---|---|---|
| Young' modulus | $E_1$ GPa | $3.2 \pm 0.2$ |
| | $E_2$ GPa | $5.9 \pm 0.9$ |
| Shear modulus | $G_1$ GPa | $1.2 \pm 0.4$ |
| | $G_2$ GPa | 0.3 |
| Poisson's ratio | $\nu_1$ | $0.33 \pm 0.02$ |
| | $\nu_2$ | $0.29 \pm 0.02$ |
| TEC | $\alpha_1$/ppm/°C | $87.1 \pm 2$ |
| | $\alpha_2$/ppm/°C | $278 \pm 31$ |

resist applications where high aspect ratio and resist to harsh etching and plating conditions are required.

To our knowledge, this is the first report on the full characterization of SU8 coatings, and the procedures of characterization used in this paper can also be used for any transversely isotropic films and coatings.

## Acknowledgment

We would like to thank the Hewlett-Packard Company, specifically Dr. Charles Schmidt for their support. We would also like to acknowledge the support of the MRSEC Central Research Facilities and the CUMIRP Program in the University of Massachusetts Amherst.

## References

1. J. M. SHAW, J. D. GELOME, N. C. LABIANCA, W. E. CONLEY and S. J. HOLMES, *IBM J. Res. Dev*. **41** (1997) 81.
2. B. EYRE, J. BLOSIU and D. WIBERG, in 11th IEEE Micro. Elec. Mech. Sys., Chicago, USA, 1995, 218.
3. A. BERTSCH, H. LORENZ and P. RENAND, in IEEE Micro. Electro. Mech. Sys., Chicago, USA, 1998, 18.
4. R. FENG and R. J. FARRIS, "Influence of Processing Conditions on the Thermal and Mechanical Properties of SU8 Negative Photoresist Coatings," *J. Micromech. Microeng.* (2002), submitted.
5. M. DESPONT, H. LORENZ, N. FAHRNI, J. BRUGGER, P. RENAUD and P. VETTIGER, in 10th, IEEE Micro. Electro. Mech. Sys., Nagoya, Japan, 1997, 518.
6. H. LORENZ, M. LAUDON and P. RENAUD, *Microelec. Eng*. **41/42** (1998) 371.
7. H. LORENZ, M. DESPONT, N. FAHRNI, N. LABIANCA, P. VETTIGER and P. RENAUD, *J. Macromech, Microeng.* **7** (1997) 121.
8. N. LABIANCA, J. GELORME and K. LEE, *Elec. Soc. Proc*. **V95-18** (1993) 386.
9. W. M. LAI, D. RUBIN and E. KREMPL, "Introduction to Continuum Mechanics" (Butterworth, Heinemann, 1996).
10. S. CHO, G. KIM, T. MCCARTHY and R. FARRIS, *Polym. Eng. Sci*. **41** (2001) 301.
11. R. FENG and R. J. FARRIS, *J. Appl. Polym. Sci.*, in print, 2002.
12. M. J. CHEN, PhD thesis, University of Massachusetts at Amherst, 1998.
13. Q. K. TONG, PhD thesis, University of Massachusetts at Amherst, 1993.
14. M. MADEN, A. JAGOTA, S. MAZUR and R. FARRIS, *J. Amer. Cerm. Soc.* **77** (1994) 625.
15. M. MADEN, PhD thesis, University of Massachusetts, 1992.
16. R. J. FARRIS, *J. Appl. Polym. Sci*. **8** (1964) 25.
17. G. RAUMANN, *Proc. Phys. Soc*. **79** (1962) 1221.
18. S. LEKHNITSKII, "Theory of Elasticity of an Anisotropic Elastic Body, Eng. Trans." (Moscow, MIR publishers, 1981).

*Received 8 March*
*and accepted 6 May 2002*